Published in final edited form as:
J Bone Miner Res. 2014 January ; 29(1): . doi:10.1002/jbmr.2007.

DYSAPOPTOSIS OF OSTEOBLASTS AND OSTEOCYTES INCREASES CANCELLOUS BONE FORMATION BUT EXAGGERATES BONE POROSITY WITH AGE

Robert L. Jilka[1], **Charles A. O'Brien**[1], **Paula K. Roberson**[1], **Lynda F. Bonewald**[2], **Robert S. Weinstein**[1], and **Stavros C. Manolagas**[1]

[1]Division of Endocrinology & Metabolism, Center for Osteoporosis and Metabolic Bone Diseases, Central Arkansas Veterans Healthcare System, 4301 W. Markham, Slot 587, University of Arkansas for Medical Sciences, Little Rock, AR 72205

[2]Department of Oral Biology, University of Missouri-Kansas City, 650 E. 25th St., Kansas City, MO 64108

Abstract

Skeletal aging is accompanied by decreased cancellous bone mass and increased formation of pores within cortical bone. The latter accounts for a large portion of the increase in non-vertebral fractures after age 65 in humans. We selectively deleted Bak and Bax, two genes essential for apoptosis, in two types of terminally differentiated bone cells: the short-lived osteoblasts that elaborate the bone matrix, and the long-lived osteocytes that are immured within the mineralized matrix and choreograph the regeneration of bone. Attenuation of apoptosis in osteoblasts increased their working lifespan and thereby cancellous bone mass in the femur. In long-lived osteocytes, however, it caused dysfunction with advancing age and greatly magnified intracortical femoral porosity associated with increased production of receptor activator of nuclear factor-κB ligand and vascular endothelial growth factor. Increasing bone mass by artificial prolongation of the inherent lifespan of short-lived osteoblasts, while exaggerating the adverse effects of aging on long-lived osteocytes, highlights the seminal role of cell age in bone homeostasis. In addition, our findings suggest that distress signals produced by old and/or dysfunctional osteocytes are the culprits of the increased intracortical porosity in old age.

Keywords

apoptosis; osteoblasts; osteocytes; bone formation; aging; cortical porosity; RANKL

INTRODUCTION

Aberrations in the rate of birth and death of osteoblasts and osteoclasts have been implicated as pathogenetic mechanisms in the development of osteoporosis (1). All osteoclasts and the majority of osteoblasts die by apoptosis. Increased osteoblast apoptosis and the associated decrease in osteoblast numbers have been implicated as key pathogenetic mechanisms for the loss of bone caused by old age, glucocorticoid excess, and sex steroid deficiency (2;3). Conversely, attenuation of osteoblast apoptosis by intermittent administration of parathyroid

Address correspondence to: Robert L. Jilka, Ph.D., Division of Endocrinology and Metabolism, University of Arkansas for Medical Sciences, 4301 W. Markham, Slot 587, Little Rock, AR 72205, 501-686-7896 (voice), 501-686-8954 (fax), rljilka@uams.edu.

DISCLOSURES

The authors state that they have no conflicts of interest.

hormone (PTH) may be, in part, responsible for the increased bone formation associated with this therapeutic modality (4).

Some of the osteoblasts that avoid death by apoptosis become osteocytes and are embedded within the mineralized matrix (5). In difference to osteoblasts which are short-lived and present on a small fraction of the bone surface, osteocytes are deployed throughout the skeleton and are long-lived. Moreover, osteocytes form an elaborate communication network with each other, endothelial cells of the bone vasculature, and cells of the bone surface and the marrow, via dendritic processes and gap junctions (6). Because of their unique features, osteocytes are ideally suited to mediate the homeostatic adaptation of bone to mechanical forces. Detection of changes in strain by osteocytes leads to changes in osteoclast and/or osteoblast recruitment by mechanisms that counteract the change in strain. Indeed, osteocytes, but not osteoblasts or their precursors, are the essential cellular sources of receptor activator of nuclear factor-κB ligand (RANKL) for osteoclast formation during bone remodeling (7;8). Osteocyte apoptosis in response to fatigue damage stimulates the production of RANKL by neighboring viable osteocytes (9;10). The local increase in RANKL in turn initiates the development of osteoclasts that remove the defective bone.

Although osteoporosis has long been attributed primarily to decreased bone mineral density (BMD), decreased BMD is only one of many changes responsible for the increase of fracture risk in patients with this condition (5;11). Indeed, a decline of BMD between the ages of 50 and 80 years accounts only for a 4-fold, as compared to an actual 30-fold, increase in the risk of hip fractures in the same time frame (11–13). Therefore, age-related changes in the bone itself clearly contribute to the increase in fracture risk independently of BMD. Considerable evidence suggests that an increase in osteocyte apoptosis and cortical porosity with advancing age are some of the seminal age-dependent mechanisms that increase fracture risk independently of BMD (5;14–17). Here, we have sought genetic evidence for a cause-and-effect relationship between the apoptosis of osteoblasts and osteocytes and skeletal homeostasis.

Apoptosis strictly depends on permeabilization of the outer mitochondrial membrane by activated Bak and Bax – two proapoptotic members of the Bcl-2 family of proteins (18;19). Activation promotes the formation of Bax and Bak homo-oligomers, as well as a small number of hetero-oligomers, within the outer mitochondrial membrane (20). These oligomers form channels that permit release of cytochrome c from mitochondria, resulting in activation of caspases that degrade critical intracellular proteins leading to cell death. However, the role of Bak and Bax in apoptosis is redundant and either one of them is sufficient to initiate the apoptosis cascade. Based on this and evidence that deletion of both Bak and Bax abrogates apoptosis in vitro and in vivo (21–23), we generated mice with germline deletion of Bak and cell type-specific deletion of Bax in mature osteoblasts and osteocytes, or osteoblast progenitors.

We show that deletion of Bak and Bax decreased mature osteoblast apoptosis and increased cancellous bone mass. Unexpectedly, however, Bak/Bax deletion also led to an increase in the number of dysmorphic osteocytes adjacent to the periosteum, increased RANKL and vascular endothelial growth factor (VEGF) expression in osteocytes, and a seven-fold increase in cortical porosity in aged mice.

MATERIALS AND METHODS

Animals

All animal procedures were approved by the Institutional Animal Care and Use Committees of the University of Arkansas for Medical Sciences and the Central Arkansas Veterans

Healthcare System. $Bak^{+/-}$;$Bax^{+/f}$ mice in a mixed background of 129 and C57BL/6 (B6) were a generous gift from Joseph Opferman (St. Jude's Children's Research Hospital, Memphis, TN)(24). These mice were interbred to obtain $Bak^{-/-}$;$Bax^{+/f}$ mice, hereafter designated $Bak^{\Delta}Bax^{+/f}$ mice. Bak^{Δ} mice in the B6 background were obtained from Jackson Labs, and intercrossed with OCN-Cre (B6/FVB background)(25) or Osx1-Cre mice (B6/129 background)(26) to obtain Bak^{Δ};OCN-Cre or Bak^{Δ};Osx1-Cre mice, hereafter designated Bak^{Δ}OCN-Cre and Bak^{Δ}Osx1-Cre mice, respectively. $Bak^{\Delta}Bax^{+/f}$ and Bak^{Δ}OCN-Cre mice were then intercrossed to obtain Bak^{Δ};$Bax^{f/f}$;OCN-Cre mice, which are designated $Bak^{\Delta}Bax^{\Delta OCN}$ mice lacking Bak and Bax in osteoblasts and osteocytes, and Bak^{Δ}OCN-Cre, Bak^{Δ}, $Bak^{\Delta}Bax^{f/f}$ littermate controls.

$Bak^{\Delta}Bax^{+/f}$ and Bak^{Δ}Osx1-Cre mice were intercrossed to obtain $Bak^{\Delta}Bax^{\Delta Osx1}$ mice lacking Bak and Bax in osteoblast progenitors, osteoblasts and osteocytes; and the littermate controls, Bak^{Δ}Osx1-Cre, Bak^{Δ}, $Bak^{\Delta}Bax^{f/f}$ mice. Dams and progeny were maintained on a doxycycline-containing diet (Bio-Serv) until 7 weeks of age, at which time the animals were switched a normal diet to induce activity of the Osx1-Cre transgene (8).

Detection of the Cre transgene was done by PCR using the following primers: Cre-for 5′-GCGGTCTGGCAGTAAAAACTATC-3′, Cre-rev 5′-GTGAAACAGCATTGCTGTCACTT-3′, product size 102 bp. For Bax gene analysis we used the following primers: Bax1-for 5'-GAATGCCAAAAGCAAACAGACC-3', Bax3-for 5'-CCACTCCCACTGTCCTTTCC-3', Bax2-rev 5'-ACTAGGCCCGGTCCAAGAAC-3'. The wild type (WT) gene was detected with Bax1-for and Bax2-rev, WT product size of 242 bp, and floxed product size of 350 bp. The deleted gene was detected with Bax3-for and Bax2-rev, product size of 300 bp.

Quantification of Bax gene deletion

Soft tissues, and whole bones were frozen immediately upon harvest. Osteocyte-enriched genomic DNA was prepared from bones treated with collagenase to remove surface cells as previously described (27). For genomic DNA isolation, bone pieces were decalcified in 14% EDTA for 1 week after collagenase digestion. Decalcified bone was then digested with proteinase K (0.5 mg/ml in 10 mM Tris, pH 8.0, 100 mM NaCl, 20 mM EDTA, and 1% SDS) at 55° C overnight. Genomic DNA from decalcified bone, and from soft tissues, was isolated by phenol/chloroform extraction and ethanol precipitation.

A custom Taqman assay was obtained from Applied Biosystems for quantifying Bax gene deletion efficiency. The following primer pair-probe sets were used to detect sequences between the loxP sites of the Bax gene: for, 5-CACCTGAGCTGACCTTGGA-3'; rev, 5-GGAGACACTCGCTCAGCTT-3'; probe, Probe, 5-Fam-TTGGTGGACGCATCCTG-NFQ-3. Relative genomic Bax DNA amount was expressed per Tert gene level, and was calculated using the ΔCt method (28).

Quantification of gene expression

Freshly dissected bones were frozen immediately in liquid N_2. Osteocyte-enriched bone was prepared by collagenase digestion before freezing (27). Osteocyte enrichment and osteoblast depletion was confirmed by the finding that, compared to intact tibial bone, the collagenase-digested bone preparations exhibited a 7-fold increase in expression of the osteocyte-specific gene Sost, and a 180-fold decrease in expression of keratocan, a gene expressed in osteoblasts but not osteocytes (29).

Total RNA was extracted from frozen bone, or from cultured cells, using Ultraspec (Biotecx Laboratories) and reverse-transcribed the RNA using the High-Capacity cDNA Archive Kit (Applied Biosystems) according to the manufacturer's instructions. The following primers

and probes for the different genes were manufactured by the TaqMan® Gene Expression Assays service (Applied Biosystems): Bax (Mm00432050_m1), cathepsin K (Mm012558622_g1), RANKL (Mm0041908-m1), OPG (Mm00435452_m1), VEGFa (Mm00437304_m1), alkaline phosphatase, Akp2 (Mm00475831_m1); and the housekeeping genes: β2-microglobulin, B2m (Mm00437762_m1), β-actin, Actb (Mm00607939_s1), mitochondrial ribosomal protein S2, Mrps2 (Mm00475529_m1); glyeraldehyde-3-phosphate dehydrogenase, Gapdh (4352932E), hydroxymethylbilane synthase, Hmbs (Mm00660262_g1), and hypoxanthine guanine phosphoribosyl transferase, Hprt1 (Mm00446968_m1). Custom made primers were used to measure osteocalcin: For, 5'-GCTGCGCTCTGTCTCTCTGA-3', Rev, 5'-TGCTTGGACATGAAGGCTTTG-3', Probe, 5'-AAGCCCAGCGGCC-3'. Relative mRNA levels were calculated using the ΔCt method (28). For bone preparations, transcripts of interest were normalized to each of the 6 housekeeping genes, and levels were expressed the geometric mean of the 6 normalized values (30). Expression of the housekeeping genes were highly correlated with each other (r=0.79–0.99).

Bone Imaging

Bone mineral density was determined by differential X-ray absorptiometry using a PIXImus densitometer (GE Lunar) as previously described (31). Micro-CT analysis was performed with a μCT40 (Scanco Medical, Basserdorf, Switzerland) on femora and vertebrae as previously described (32;33), following fixation and transfer to 100% ethanol. Calibration and quality control was done weekly using five density standards, and spatial resolution was verified monthly using a tungsten wire rod. Beam-hardening correction was based on the calibration records. Corrections were made for 200 mg/cm^3 hydroxyapatite for all energies. Over the past 3 years, the coefficient of variation for the fifth density standard was 0.97% (787 ± 7.6 SD mg HA/cm^3) and for rod volume was 2.18% (0.0642 ± 0.0014 SD cm^3).

For trabecular bone determinations, the distal femur was scanned from the boundary between the growth plate and metaphysis towards the diaphysis to obtain 151 slices (12 μm/slice). The 4th lumbar vertebra was scanned from the rostral growth plate to the caudal growth plate to obtain 233 slices. In both bones, analyses were performed on contours of the cross sectional acquired images drawn to exclude the primary spongiosa and cortex. Micro-CT measurements of cancellous bone architecture were based on the direct transformation (DT) approach as recommended by Scanco, and were expressed in 3D nomenclature (34). An animation of sequential 85 eight μm thick micro-CT images of the diaphysis of 22-month-old Bak$^{\Delta}$Bax$^{\Delta OCN}$ mice was made using using the Scanco 3D program and Windows Movie Maker 2.6.

For cortical bone porosity measurements, femora were scanned from a point immediately distal to the third trochanter to the beginning of the distal growth plate at medium resolution (nominal isotropic voxel size = 12 μm). Scans were integrated into 3D voxel images, 1024 × 1024 pixel matrices for each individual planar stack. A Gaussian filter (sigma = 0.8, support = 1) was applied to all analyzed scans. Key parameters were x-ray tube potential = 55 kVp, x-ray intensity = 145 μA, integration time = 200 ms, and threshold = 200 mg/cm^3. To obtain inverse mirco-CT images, the normal 3D image was re-analyzed with an image processing script that reassigns void spaces with the higher threshold relative to the bone to invert the image based on material density. A second image processing script (“peel-iter”) was used to eliminate false voids caused by imperfect wrap of the contours to the bone surface. The “cl_image” processing language script was used to obtain lists of the number of pores and their respective sizes. Per communication from Scanco Medical, the minimal resolution of porosity is 8192 μm^3 (2 × 10% of the modulation transfer function). To reduce measurement error and avoid inclusion of canalicular space, which ranges from 10,000 to 28,000 μm^3

(35), pores with volumes less than 31,104 μm^3 (18 voxels) were excluded in calculation of porosity.

Histology and Histomorphometry

Mice were injected with tetracycline (30 mg/kg) at 6 and 2 days before euthanasia. Bones were fixed in Millonig's formalin, and embedded nondecalcified in methyl methacrylate; or decalcified in EDTA and embedded in paraffin. Tetracycline labeling and osteoclast number were quantified on 5 μm thick longitudinal sections of nondecalcified femora using a computer and digitizer tablet (Osteomeasure version XP 3.1, Osteometrics Inc., Atlanta, GA) interfaced to a Zeiss Axioscope with a drawing tube attachment. Cancellous measurements in the femur were done on secondary spongiosa. Intracortical measurements were performed on one entire cortex, bounded by each growth plate. The endosteal surface was excluded. Data are reported using the nomenclature recommended by the American Society for Bone and Mineral Research (36). Unadjusted values of bone perimeter and osteoclast perimeter were also reported to indicate the increased perimeter available in $Bak^{\Delta}Bax^{\Delta OCN}$ mice.

For histologic determination of osteocyte morphology and cortical porosity, nondecalcified sections were stained with toluidine blue. Cortical bone area in the periosteal or endosteal zone, and intracortical pores, were quantified by histomorphometry. Apoptotic cells in decalcified bone sections were visualized by in-situ end-labeling (ISEL) using the FragEL DNA fragmentation kit (EMD, San Diego, CA). Osteoclasts were visualized by staining for tartrate-resistant acid phosphatase (TRAPase) using napthol AS-MX and Fast Red TR salt (Sigma-Aldrich, St. Louis, MO).

Photomicrographs of osteocytes in nondecalcified sections were taken with a Zeiss Axioplan 2 motorized imaging microscope using a 100x Plan-Apochromat oil lens with a 1.40 numerical aperture and a 1.6x Optovar magnifier (Carl Zeiss, Thornwood, NY). From 3 to 8 images were acquired at 200–400 nm intervals using an extended focus and the image set was compiled from the Z-stack using Axiovision (Carl Zeiss). Tone balance of the photomicrographs was obtained with a uniformly applied color balance layer (Adobe Photoshop CS2 v9.0.2, Abode Systems, San Jose, CA).

Backscattered scanning electron microscopy (BSEM) was performed as previously described (37). Briefly, gold palladium-coated nondecalcified bone sections were examined using an FEI/Philips XL30 field emission environmental SEM. Accelerated voltage in the range 15–25 KeV was used for the secondary and backscattered electron imaging. Nondecalcified sections were acid etched with 37% phosphoric acid for 12 seconds, then washed with distilled water and commercial bleach as described previously (38). SEM was used to image completely exposed resin-casted osteocytic lacunae and canaliculi.

Cell culture

Femoral bone marrow aspirates were pooled from 3–5 mice per genotype, and cultured at 3×10^6 cells per 10 cm^2 well in α-MEM supplemented with 10% FBS and 1 mM ascorbate-2-glycerophosphate. One half of the medium was replaced every 5 days. After 25 days, RNA was obtained for qPCR, or cells were stained with von Kossa to visualize mineral deposition. For apoptosis determination, cells were cultured at 5×10^6 cells per 12 well plate under as above for 15 days. Then, basal and camptothecin-induced apoptosis was determined by measurement of caspase-3 activity (39).

Statistics

All values are reported as the mean ± s.d. The SigmaPlot (SPSS Science) and SAS software packages were used for statistical analyses. Student's 2-tailed t-test or one way ANOVA was used to detect treatment effects. If necessary, data were logarithmically transformed to achieve normal distribution. The Holm-Sidak method was used to detect significant differences among treatment groups following ANOVA. In some experiments, values from littermate controls were combined after first determining that there were no significant differences among genotypes. Sequential BMD data were analyzed using random coefficients models. Fixed effects were included for the intercept, genotype, age (treated as a continuous variable), group*age, age^2, group*age^2, and baseline BMD. Random effects for the intercept, age, and age^2 coefficients allowed the association of repeated determinations made with the same animal to be measured. An unstructured covariance structure was assumed.

RESULTS

Lack of Bak and Bax reduces osteoblast and osteocyte apoptosis and increases bone mass

Deletion of Bak and Bax in osteoblasts and osteocytes was accomplished by intercrossing $Bak^{-/-};Bax^{+/f}$ mice with $Bak^{-/-}$ mice bearing Cre recombinase under the control of osteocalcin gene regulatory elements ($Bak^{-/-}$;OCN-Cre mice). The OCN-Cre transgene becomes active in replicating osteoblast progenitors just prior to their development into matrix synthesizing osteoblasts (25). $Bak^{-/-};Bax^{f/f}$;OCN-Cre mice (hereafter designated $Bak^{\Delta}Bax^{\Delta OCN}$ mice) as well as Bak^{Δ}, $Bak^{\Delta}Bax^{f/f}$, and Bak^{Δ}OCN-Cre littermate controls, were born at the expected Mendelian ratios and did not exhibit discernible abnormalities at birth. Deletion of the Bax conditional allele was detected in cortical bone, but not in brain, liver or spleen of $Bak^{\Delta}Bax^{\Delta OCN}$ mice (Figure 1A). Osteoblastic cell cultures established from femoral bone marrow aspirates from $Bak^{\Delta}Bax^{\Delta OCN}$ mice exhibited reduced expression of Bax and attenuation of camptothecin-induced apoptosis, as compared to cells cultured from littermate controls (Figure 1B).

Deletion of Bak and Bax caused a progressive increase in femoral bone mineral density (BMD) in a cohort of female mice (Figure 1C). Specifically, femoral BMD of $Bak^{\Delta}Bax^{\Delta OCN}$ mice was greater than that of the controls beginning at 6 months of age, and remained so up to 13 months of age. However, the higher BMD of the $Bak^{\Delta}Bax^{\Delta OCN}$ mice declined to the control values by 18 months of age. The femoral BMD of Bak^{Δ}OCN-Cre mice was indistinguishable from Bak^{Δ} and $Bak^{\Delta}Bax^{f/f}$ mice, indicating that the increased femoral BMD of the $Bak^{\Delta}Bax^{\Delta OCN}$ was indeed due to the deletion of Bax rather than a nonspecific effect of Cre recombinase (40). Femoral bone growth was unaffected by lack of Bak and Bax as femoral length and the morphology of the growth plate of 2-month-old $Bak^{\Delta}Bax^{\Delta OCN}$ mice was identical to that of littermate controls (Supplementary Figure 1A,B). Both spinal BMD and body weight of $Bak^{\Delta}Bax^{\Delta OCN}$ mice was indistinguishable from controls at all ages examined (Figure 1D,E).

We next determined whether abrogation of apoptosis in osteoblast progenitors would augment the skeletal phenotype produced by Bax deletion in mature cells alone. To do this, we used transgenic mice expressing Cre recombinase under the control of Osterix 1 (Osx1) regulatory elements. In this Osx1-Cre deleter strain, the Cre recombinase is expressed in committed osteoblast progenitors (26). Expression of the Cre transgene is suppressed by doxycycline (26) and was induced in our study by removal of animals from a doxycycline diet at 7 weeks of age. Bax DNA was reduced in femurs of $Bak^{\Delta}Bax^{\Delta Osx1}$ mice (Figure 1F). Moreover, a cohort of female $Bak^{\Delta}Bax^{\Delta Osx1}$ mice exhibited a similar pattern of accrual, and

subsequent loss, of femoral bone mass as the $Bak^{\Delta}Bax^{\Delta OCN}$ mice (Figure 1G). Spinal BMD and body weight were not affected in the $Bak^{\Delta}Bax^{\Delta Osx1}$ mice (Figure 1H,I).

Lack of Bak and Bax increases femoral cancellous bone and magnifies the age-related development of cortical porosity

As expected, the prevalence of osteoblast apoptosis was reduced in cancellous bone of 8-month-old $Bak^{\Delta}Bax^{\Delta OCN}$ mice, compared to controls (Figure 2A). Cortical osteocyte apoptosis was also reduced. Complete abrogation of osteoblast and osteocyte apoptosis was not achieved, probably due to retention of Bax expression in some cells and/or non-specific ISEL staining. In any event, osteoblast number was increased by more than 2-fold as measured in the same femoral sections from $Bak^{\Delta}Bax^{\Delta OCN}$ mice (Figure 2B), and this effect was associated with an increase in cancellous bone area (Figure 2C). Attenuation of osteoblast apoptosis also resulted in an increase in osteocyte density (Figure 2D), as previously observed in mice with reduced osteoblast apoptosis following daily injections of PTH (41).

Three-dimensional (3D) microcomputed tomography (micro-CT) images of femurs from $Bak^{\Delta}Bax^{f/f}$ mice showed that cancellous bone was largely confined to the metaphysis in 3- and 8-month-old mice, respectively; and had practically disappeared by 22 months at of age (Figure 2E), consistent with earlier findings on the impact of aging on murine cancellous bone (33;42). In contrast, cancellous bone was present throughout the marrow of 3-, 8- and 22-month-old $Bak^{\Delta}Bax^{\Delta OCN}$ mice (Figure 2E). A similar pattern of femoral cancellous bone retention with age was also found in 7- and 21-mo-old $Bak^{\Delta}Bax^{\Delta Osx1}$ mice (Figure 3A). Cancellous bone architecture was determined in the distal femoral metaphysis on a group of males and females at 3 months of age, males at 7–8 months of age, and females at 21–22 months of age. Cancellous bone volume per tissue volume (BV/TV) was higher in $Bak^{\Delta}Bax^{\Delta OCN}$ than in controls at 3, 8 and 22 months of age (Figure 2F). Similarly, $Bak^{\Delta}Bax^{\Delta Osx1}$ mice exhibited higher BV/TV at 7 and 21 months of age (Figure 3B). The finding of a similar increase in femoral cancellous bone mass in both $Bak^{\Delta}Bax^{\Delta OCN}$ and $Bak^{\Delta}Bax^{\Delta Osx1}$ mice indicates that this phenomenon was indeed due to the abrogation of apoptosis in mature cells alone.

The increased cancellous bone volume could be accounted for by increased trabecular number, decreased trabecular separation, and increased trabecular connectivity in 3- and 22-month old $Bak^{\Delta}Bax^{\Delta OCN}$ mice (Figure 2G,H,J), and in 21-month-old female $Bak^{\Delta}Bax^{\Delta Osx1}$ mice (Figure 3C,D,F). In male mice examined at 8 months of age, there was only a small increase in trabecular number and a small decrease in trabecular separation. These changes were statistically significant in $Bak^{\Delta}Bax^{\Delta Osx1}$ mice (Figure 3C,D) but not $Bak^{\Delta}Bax^{\Delta OCN}$ mice (Figure 2G,H). The reason for the discrepancy between the large change in BV/TV as compared to the small changes in Tb.N and Tb.Sp in 7–8-month-old males lacking Bak and Bax is unclear, and requires further investigation. Trabecular thickness was unaffected by lack of Bak and Bax at all ages examined in both the OCN-Cre (Figure 2I), and the Osx1-Cre (Figure 3E) models.

Vertebral cancellous bone volume was unaffected in $Bak^{\Delta}Bax^{\Delta OCN}$ mice at 3 and 8 months of age, and in 7 month old $Bak^{\Delta}Bax^{\Delta Osx1}$ mice (Supplementary Figure 2). Although there was an increase in mean BV/TV in 21–22 month old Bak/Bax-deficient mice as compared to controls, the change was not statistically significant. These findings are consistent with the lack of an effect of the deletion of Bak and Bax on spinal BMD in both strains (Figure 1D,H).

In difference to the pronounced cancellous bone phenotype of femora of Bak/Bax deficient mice, earlier attempts to abrogate apoptosis by over-expression of the anti-apoptotic protein

Bcl-2 in osteoblasts caused either a transient increase or no change in femoral cancellous bone mass, probably due to an inhibitory effect of high Bcl-2 levels on osteoblast differentiation (43;44). However, deletion of Bak and Bax had no such effect (Supplementary Figure 3). As expected for osteoblasts with a prolonged lifespan, mineral deposition and expression of alkaline phosphatase and osteocalcin was significantly higher in cultures of bone marrow-derived osteoblastic cells from $Bak^{\Delta}Bax^{\Delta OCN}$ mice, compared to cells cultured from control mice.

Strikingly, micro-CT images revealed far more intracortical pores, or voids, in femora of 22-month-old female $Bak^{\Delta}Bax^{\Delta OCN}$ mice (Figure 2E, and enlarged images in Figure 4A) and 21-month-old $Bak^{\Delta}Bax^{\Delta Osx1}$ mice (Figures 3A and 4A), as compared to age-matched control mice. The presence of intracortical voids was confirmed in both the femur and tibia of aged female $Bak^{\Delta}Bax^{\Delta Osx1}$ mice by histology (Figure 4B). In some areas, trabecularization of the endocortical bone had occurred, while in others the interior of the cortex contained voids of various size (Figure 4C). Very large voids were sometimes associated with cortical expansion into the marrow space, along with the formation of new endosteal boundary (Figure 4A,C). As a result, large porous areas (e.g. right panel of Fig. 4C) appeared to be located in the middle of the cortex. Lack of a well-defined endosteal boundary prevented accurate determination of cortical thickness in aged Bak/Bax-deficient mice. However, in 3- and 7–8-month-old mice lacking Bak and Bax, which had an intact endosteal boundary, femoral cortical thickness was indistinguishable from controls (Supplementary Figure 1C).

The percentage of cortical bone occupied by voids (porosity), measured in histologic sections, was 4–7-fold higher in femora and tibiae from $Bak^{\Delta}Bax^{\Delta OCN}$ and $Bak^{\Delta}Bax^{\Delta Osx1}$ mice as compared to controls (Table 1). Femoral porosity of Bak^{Δ}OCN-Cre mice varied more than all the other controls, but this phenomenon was not seen in tibiae, excluding the possibility of a Cre effect. Because the cortical porosity phenotype was practically identical in $Bak^{\Delta}Bax^{\Delta OCN}$ and $Bak^{\Delta}Bax^{\Delta Osx1}$ mice, bones from either genotype were used interchangably in the subsequent work.

Inverse 3D micro-CT images revealed that the intracortical pores were distributed throughout the distal portion of the femur of 21-month-old $Bak^{\Delta}Bax^{\Delta Osx1}$ mice, whereas pores were largely located in the metaphyseal cortex of $Bak^{\Delta}Bax^{f/f}$ controls (Figure 4D). Quantification of the inverse 3D images gives a more accurate measure of porosity than that obtained using a single histologic section. Using this approach, we found that porosity of femoral bone of aged $Bak^{\Delta}Bax^{\Delta Osx1}$ mice was 7-fold greater than that of controls due to an increase in pore size (Figure 4E). The number of pores, however, was reduced due to coalescence of small pores into larger ones. Indeed, in a series of 8 μm thick cross-sectional micro-CT images taken at the femoral mid-diaphysis of a 22-month-old $Bak^{\Delta}Bax^{\Delta OCN}$ mouse, small pores were frequently contiguous with larger pores (Supplementary Video 1).

Pores were rare in femora from 3-month-old Bak and Bax deficient mice or controls, whether viewed in longitudinal sections (not shown), 3D micro-CT images (Supplementary Figure 4), or in inverse 3D micro-CT images (Figure 4F). The femoral cortical porosity of 3-month-old control mice was approximately 1.5% and increased to 6% by 21 months of age (Figure 4G and 4E, respectively), consistent with earlier evidence that cortical porosity is a feature of old age in rodents (45–47). Nevertheless, even at 3 months of age, cortical porosity was 17% higher in $Bak^{\Delta}Bax^{\Delta OCN}$ mice than in control mice, due to a small increase in pore size (Figure 4G).

In contrast to the situation in femoral bone, porosity was not observed in histologic sections or microCT images of vertebral cortical bone of aged Bak/Bax-deficient mice or controls (data not shown).

The age-related increase in cortical porosity is due to increased intracortical bone remodeling

Backscattered scanning electron microscopy (BSEM) of the femoral diaphyseal cortex of 22-month-old control mice revealed two distinct zones separated by a mineral-rich boundary (Figure 5A). The endosteal zone contained highly mineralized scalloped tidemarks that mark previous episodes of bone remodeling (48;49). In contrast, the periosteal zone had a lamellar structure, and lacked markings of remodeling activity. Cortical voids in femora from 22-month-old $Bak^{\Delta}Bax^{\Delta OCN}$ mice were largely restricted to the endosteal zone, and rarely invaded the periosteal zone (Figure 5B). Moreover, the porous endosteal zone of these mice exhibited areas of bright mineralized matrix, reflecting older bone, juxtaposed to areas of dimmer newly formed bone. These features are diagnostic of recent remodeling activity (48).

Cortical voids in both the aged $Bak^{\Delta}Bax^{\Delta OCN}$ mice and the control mice contained osteoclasts as well as osteoblasts adjacent to osteoid matrix, blood vessels, and cells indistinguishable from those inhabiting the bone marrow (Figure 6A). In addition, surfaces outlining the voids were labeled by tetracycline, confirming active intracortical remodeling. Expression of cathepsin K and osteocalcin – markers of osteoclasts and osteoblasts, respectively – was increased in tibiae of $Bak^{\Delta}Bax^{\Delta OCN}$ mice, as compared to control mice (Figure 6B). Moreover, expression of RANKL was increased, whereas expression of the RANKL antagonist osteoprotegerin (OPG) was unchanged, compared to controls. In line with the presence of blood vessels in the voids and a higher porosity in $Bak^{\Delta}Bax^{\Delta OCN}$ mice, the expression of VEGF was also increased in these mice. The increase in RANKL and VEGF transcripts was confirmed in osteocyte-enriched humeri from $Bak^{\Delta}Bax^{\Delta Osx1}$ mice (Figure 6C), indicating that osteocytes are the principal source of the increased RANKL and VEGF.

Histomorphometric measurements showed that void area, intracortical bone perimeter, and osteoclast perimeter were increased in the endocortical zone of the femoral cortex of aged $Bak^{\Delta}Bax^{\Delta OCN}$ mice compared to controls (Table 2). These measurements reflect the increase in cortical porosity, and indicate that osteoclastic erosion of the cortex is responsible. However, when expressed per mm of intracortical bone surface, osteoclast number was not affected by Bak/Bax deficiency. Nor were dynamic indices of bone remodeling, including mineralizing surface, mineral apposition rate, and bone formation rate. Taken together, these findings demonstrate an increase in the amount of intracortical bone engaged in remodeling in aged Bak/Bax deficient mice. The cancellous bone perimeter and area were also increased in aged $Bak^{\Delta}Bax^{\Delta OCN}$ mice, consistent with the micro-CT findings. The paucity of cancellous bone prevented precise determination of the number of osteoclasts at this site. Nevertheless, there was sufficient tetracycline labeling in the limited amount of bone available to show that, as in the intracortical pores, dynamic indices of cancellous bone remodeling were unaffected by Bak/Bax deficiency in these aged mice.

Serum levels of Ca, Pi and PTH, as well as 1α-hydroxylase transcripts in the kidney (a PTH target gene), were similar in $Bak^{\Delta}Bax^{\Delta Osx1}$ mice and littermate controls (Table 3). Moreover, there was no evidence of the marrow fibrosis often seen in conditions of excess PTH (Figure 4B,C). These findings suggest that a local, rather than a systemic, stimulus was responsible for the increased porosity in aged $Bak^{\Delta}Bax^{\Delta OCN}$ mice.

The increased cortical porosity in aged $Bak^{\Delta}Bax^{\Delta OCN}$ mice is associated with dysmorphic osteocytes

The majority of cortical osteocytes in 22-month-old $Bak^{\Delta}Bax^{\Delta OCN}$ or littermate control mice occupied the entire lacunar space and had prominent nuclear profiles containing nucleoli. (Figure 7A). Nonetheless, some osteocytes displayed dysmorphic features, including condensed cytoplasm and pyknotic nucleus without nucleoli. The prevalence of dysmorphic osteocytes was higher in the periosteal zone of both control and $Bak^{\Delta}Bax^{\Delta OCN}$ mice, as compared to the endosteal zone (Figure 7B). Strikingly, dysmorphic osteocytes in the periosteal zone were more numerous in $Bak^{\Delta}Bax^{\Delta OCN}$ mice compared to the periosteal zone of controls. Moreover, there was a correlation between the prevalence of dysmorphic periosteal zone osteocytes and the extent of cortical porosity ($r=0.6$, $p<0.02$), suggesting a cause and effect relationship.

Attenuation of apoptosis by overexpression of Bcl-2 decreases osteocyte viability, most likely by inhibiting canalicular development (44). Thus, the dysmorphic osteocytes in Bak/Bax-deficient mice could be due to an increase in free Bcl-2 protein, which would normally bind to Bax and Bak and prevent apoptosis. However, the morphology of the lacunae and canaliculi of cortical osteocytes, visualized by acid-etch SEM, of 22-mo-old $Bak^{\Delta}Bax^{\Delta OCN}$ mice was indistinguishable from that of controls, thus excluding this possibility (Figure 7C).

DISCUSSION

In the work presented herein, we generated mice with targeted deletion of Bak and Bax – two genes indispensable for apoptosis – in mature osteoblasts and osteocytes, or in osteoblast progenitors. We found that both of these models exhibited increased cancellous bone mass that extended throughout the femoral bone marrow cavity, as compared to control mice, in which cancellous bone mass was limited to the metaphysis. The increased cancellous bone mass in the Bak/Bax-deficient mice could fully account for the progressive increase in femoral BMD up to 13 months of age. Unexpectedly, by 22 months of age, these mice also had a 7-fold greater pore formation in the endocortical (inner) envelope of long bone cortices. These pores were present throughout the cortex of the Bak/Bax-deficient female mice, whereas pores were limited to the metaphysis in control mice. The dramatic increase in cortical porosity of Bak/Bax deficient mice could account for the decline in femoral BMD between 13 and 21–22 months of age.

The increased porosity of the Bak/Bax-deficient mice was accompanied by increased osteoclast formation that was most likely due to increased expression of RANKL and VEGF in osteocytes, albeit we cannot exclude the possibility that cells at other stages of osteoblast differentiation also contributed to the increase in these cytokines. In addition to osteoclasts, the pores contained osteoblasts, bone marrow cells, and blood vessels as well as bone surfaces exhibiting histologic features of bone turnover. Notably, the increased porosity in the Bak/Bax-deficient mice in the endocortical envelope was associated with an increase in the number of dysmorphic osteocytes in the adjacent periosteal compartment of the femoral cortex.

These findings demonstrate that abrogation of apoptosis, and the consequent prolongation of the working lifespan of short-lived osteoblasts, is sufficient to increase femoral cancellous bone mass. In addition, deletion of Bak and Bax exaggerates the adverse effects of aging on the function of long-lived cortical osteocytes, most likely by interfering with compensatory adaptations to age-associated stressors. Hence, signals from dysfunctional osteocytes, including increased production of RANKL and VEGF, may be the culprits of the age-associated increase in cortical porosity.

Osteoblast number and bone formation rate in murine bone decrease with age, resulting in the disappearance of most of the metaphyseal cancellous compartment of long bones by 12 months (33;42). Deletion of Bak and Bax from committed osteoblast progenitors in $Bak^{\Delta}Bax^{\Delta Osx1}$ mice did not result in a further increase in femoral cancellous bone than that seen in $Bak^{\Delta}Bax^{\Delta OCN}$ mice, indicating that abrogation of apoptosis in the mature cells was responsible for the phenotype in both models. Moreover, the increased functional life span of short-lived osteoblasts in the Bak/Bax-deficient models was associated with retention of cancellous bone in the bone marrow up to 21–22 months of age. This observation suggests that the age-related increase in osteoblast apoptosis noted in our earlier studies (2) contributes to age-related bone loss.

Taken together, these findings provide genetic evidence that attenuation of osteoblast apoptosis can indeed increase the working lifespan of these matrix synthesizing cells in the femur. This evidence bolsters our earlier contention that prolongation of osteoblast life span contributes to the anabolic effect of intermittent administration of PTH (4;41;50). However, deletion of Bak and Bax was not sufficient to increase trabecular thickness – a hallmark of the anabolic effect of intermittent PTH on the skeleton. Therefore, this therapy must involve additional mechanisms, such as stimulation of Wnt signaling leading to increased osteoblastogenesis (51;52).

We have previously noted equivalent levels of apoptotic osteoblasts in both femoral and vertebral cancellous bone (50). Nevertheless, neither $Bak^{\Delta}Bax^{\Delta OCN}$ nor $Bak^{\Delta}Bax^{\Delta Osx1}$ mice exhibited an increase in vertebral cancellous bone mass, albeit there was a non-significant increase in vertebral cancellous bone volume in 21- and 22-mo-old Bak/Bax-deficient mice. Lack of statistical power may have compromised our ability to detect a subtle effect at this site. Recent studies of ours have shown that OCN-Cre and Osx1-Cre have similar activity in femoral and vertebral bone (53), making it unlikely that lack of a vertebral phenotype is due to ineffective deletion of Bax. Another possibility is that osteoblast apoptosis plays a less important role in the formation and maintenance of vertebral trabecular bone than femoral trabecular bone. Indeed, there are fundamental differences in the factors that determine osteoblast number and remodeling balance at these two sites as evidenced by the more rapid rate of loss of femoral versus vertebral trabecular bone between 2 and 20 months of age (33). Our findings suggest that osteoblast apoptosis may be one of them.

Deletion of Bak and Bax also did not affect the formation of femoral cortical bone during growth. This finding is consistent with earlier studies of ours that, unlike cancellous osteoblasts, apoptosis rarely if ever occurs in periosteal osteoblasts (54). We therefore conclude that osteoblast apoptosis does not play a role in the development of cortical bone.

The highest proportion of dysmorphic osteocytes was found in the periosteal zone of the femoral cortex of aged Bak/Bax deficient mice. Several lines of earlier evidence strongly suggest that these are the oldest osteocytes of cortical bone. Indeed, in human cortical bone, the further away osteocytes are from the endosteal surface, the lower the probability that they will be removed by remodeling. Left undisturbed by remodeling long enough, the intrinsic lifespan of cortical osteocytes is exceeded (55). In line with this evidence and the contention that the periosteal zone osteocytes in our studies were the oldest, we found no signs of current or past remodeling in the periosteal zone of the murine femoral cortex. Exposure of Bak/Bax-deficient embryonic fibroblasts to a pro-apoptotic stimulus activates autophagy-mediated death, which does not begin to occur until several days later (56). Although the fate Bak/Bax-deficient osteocytes in the periosteal zone is unknown, it is likely that abrogating their ability to die by apoptosis increased their lifespan beyond their intrinsic limit. These osteocytes are therefore older and perhaps more sensitive to the effects of aging as compared to the same population of cells in the control mice. As a result, Bak/Bax-

deficient osteocytes in the periosteal zone are more likely to accumulate damage during aging (5).

Osteocyte-enriched preparations of long bones from aged female Bak- and Bax-deficient mice expressed higher levels of RANKL and VEGF. This finding is reminiscent of the observation that osteocyte apoptosis in response to fatigue damage triggers intracortical remodeling by stimulating the local production of RANKL and VEGF by neighboring viable osteocytes (9). Hence, apoptotic, aged, and/or dysfunctional osteocytes of the periosteal region of the femur may trigger similar signals alerting viable osteocytes in their vicinity, or perhaps in the endosteal region of the cortex, to initiate intracortical remodeling that leads to the development of cortical porosity (57). These considerations lead us to propose that the increased femoral porosity of Bak/Bax-deficient mice is due to exaggeration of the normal effect of aging on osteocyte function due to artificial prolongation of the life span of damaged osteocytes, leading to increased numbers of RANKL- and VEGF-expressing osteocytes. The critical pathogenetic role of RANKL in this process is strongly supported by evidence that osteocytes are the major source of this cytokine (7;8), and that administration of soluble RANKL to mice stimulates bone remodeling that is unbalanced in favor of bone resorption, and causes femoral cortical porosity (58–60). Further studies are needed to determine whether Bak/Bax-deficiency indeed exaggerates an ongoing age-related process, or whether it unleashes a novel pathway leading to cortical porosity.

In summary, our results reveal that interference with Bax and Bak in short- versus long-lived bone cells has profound, but diametrically opposite biological implications for the homeostasis of femoral bone: bone anabolism in the former, and catabolism in the latter caused by exaggeration of the adverse effects of aging. These insights not only validate the notion that altered osteoblast apoptosis is a critical determinant of cancellous bone mass and a rational target of anabolic bone therapies (61). They also suggest that distress signals produced by old and/or dysfunctional osteocytes in cortical bone are the culprits of the intracortical porosity caused by old age in humans. Furthermore, the demonstration of increased bone mass by artificial prolongation of the inherent lifespan of short-lived osteoblasts, but exaggeration of the adverse effects of aging on long-lived osteocytes, highlights the important role of cell age in bone homeostasis.

Supplementary Material

Refer to Web version on PubMed Central for supplementary material.

Acknowledgments

This work was supported by the Department of Veterans Affairs, the Biomedical Laboratory Research and Development Service of the VA Office of Research and Development (Research Career Scientist award and I01 BX000514 to R.L.J., I01 BX000436 to R.S.W., I01 BX000294 to C.A.O., and I01 BX001405 to S.C.M.); by the National Institutes of Health (P01 AG013918 to S.C.M., and P01 AR46798 to L.F.B.); by the UAMS Translational Research Institute (1UL1RR029884); and by Tobacco Settlement Funds provided by the UAMS College of Medicine. The authors thank Maria Almeida and Haibo Zhao for helpful discussions. We also thank A. DeLoose, L. Climer, M. Palmieri, K. Vyas, S. Berryhill, T. Chambers, and A. Warren, and A. Xie for their contributions to this work. R.L.J designed and directed the experiments. P.K.R. performed statistical analysis of sequential BMD measurements, and provided statistical advice. R.S.W., C.A.O., L.F.B., S.C.M. and R.L.J. contributed methods and advice, and discussed the results. R.L.J. and S.C.M. wrote the manuscript.

Reference List

1. Manolagas SC. Birth and death of bone cells: basic regulatory mechanisms and implications for the pathogenesis and treatment of osteoporosis. Endocr Rev. 2000; 21:115–137. [PubMed: 10782361]

2. Almeida M, Han L, Martin-Millan M, Plotkin LI, Stewart SA, Roberson PK, Kousteni S, O'Brien CA, Bellido T, Parfitt AM, Weinstein RS, Jilka RL, Manolagas SC. Skeletal involution by age-associated oxidative stress and its acceleration by loss of sex steroids. J Biol Chem. 2007; 282:27285–27297. [PubMed: 17623659]
3. Weinstein RS, Jilka RL, Parfitt AM, Manolagas SC. Inhibition of osteoblastogenesis and promotion of apoptosis of osteoblasts and osteocytes by glucocorticoids: potential mechanisms of their deleterious effects on bone. J Clin Invest. 1998; 102:274–282. [PubMed: 9664068]
4. Jilka RL. Molecular and cellular mechanisms of the anabolic effect of intermittent PTH. Bone. 2007; 40:1434–1446. [PubMed: 17517365]
5. Manolagas SC, Parfitt AM. What old means to bone. Trends in Endocrinology & Metabolism. 2010; 21:369–374. [PubMed: 20223679]
6. Bonewald LF. The amazing osteocyte. J Bone Miner Res. 2011; 26:229–238. [PubMed: 21254230]
7. Nakashima T, Hayashi M, Fukunaga T, Kurata K, Oh-Hora M, Feng JQ, Bonewald LF, Kodama T, Wutz A, Wagner EF, Penninger JM, Takayanagi H. Evidence for osteocyte regulation of bone homeostasis through RANKL expression. Nat Med. 2011; 17:1231–1234. [PubMed: 21909105]
8. Xiong J, Onal M, Jilka RL, Weinstein RS, Manolagas SC, O'Brien CA. Matrix-embedded cells control osteoclast formation. Nat Med. 2011; 17:1235–1241. [PubMed: 21909103]
9. Kennedy OD, Herman BC, Laudier DM, Majeska RJ, Sun HB, Schaffler MB. Activation of resorption in fatigue-loaded bone involves both apoptosis and active pro-osteoclastogenic signaling by distinct osteocyte populations. Bone. 2012; 50:1115–1122. [PubMed: 22342796]
10. Jilka RL, Noble B, Weinstein RS. Osteocyte apoptosis. Bone. 2013; 54:264–271. [PubMed: 23238124]
11. Manolagas SC. From estrogen-centric to aging and oxidative stress: A revised perspective of the pathogenesis of osteoporosis. Endocr Rev. 2010; 31:266–300. [PubMed: 20051526]
12. Hui SL, Slemenda CW, Johnston CC Jr. Age and bone mass as predictors of fracture in a prospective study. J Clin Invest. 1988; 81:1804–1809. [PubMed: 3384952]
13. Kanis JA, Borgstrom F, De LC, Johansson H, Johnell O, Jonsson B, Oden A, Zethraeus N, Pfleger B, Khaltaev N. Assessment of fracture risk. Osteoporos Int. 2005; 16:581–589. [PubMed: 15616758]
14. Zebaze RM, Ghasem-Zadeh A, Bohte A, Iuliano-Burns S, Mirams M, Price RI, Mackie EJ, Seeman E. Intracortical remodelling and porosity in the distal radius and post-mortem femurs of women: a cross-sectional study. Lancet. 2010; 375:1729–1736. [PubMed: 20472174]
15. Nicks KM, Amin S, Atkinson EJ, Riggs BL, Melton LJ III, Khosla S. Relationship of age to bone microstructure independent of areal bone mineral density. J Bone Miner Res. 2012; 27:637–644. [PubMed: 22095490]
16. Bjornerem A, Ghasem-Zadeh A, Zebaze R, Bui M, Wang X, Hopper JL, Seeman E. Cortical porosity and bone loss predate menopause. J Bone Miner Res. 2012; 27:S67.
17. Bala Y, Zebaze R, Ghasem-Zadeh A, Peterson J, Amin S, Melton LJ, Khosla S, Seeman E. Osteoporosis is not enough: cortical porosity identifies women with distal forearm fractures. J Bone Miner Res. 2012; 27:S42.
18. Galluzzi L, Vitale I, Abrams JM, Alnemri ES, Baehrecke EH, Blagosklonny MV, Dawson TM, Dawson VL, El-Deiry WS, Fulda S, Gottlieb E, Green DR, Hengartner MO, Kepp O, Knight RA, Kumar S, Lipton SA, Lu X, Madeo F, Malorni W, Mehlen P, Nunez G, Peter ME, Piacentini M, Rubinsztein DC, Shi Y, Simon HU, Vandenabeele P, White E, Yuan J, Zhivotovsky B, Melino G, Kroemer G. Molecular definitions of cell death subroutines: recommendations of the Nomenclature Committee on Cell Death 2012. Cell Death Differ. 2012; 19:107–120. [PubMed: 21760595]
19. Shamas-Din A, Brahmbhatt H, Leber B, Andrews DW. BH3-only proteins: Orchestrators of apoptosis. Biochim Biophys Acta. 2011; 1813:508–520. [PubMed: 21146563]
20. Dewson G, Ma S, Frederick P, Hockings C, Tan I, Kratina T, Kluck RM. Bax dimerizes via a symmetric BH3:groove interface during apoptosis. Cell Death Differ. 2012; 19:661–670. [PubMed: 22015607]

21. Takeuchi O, Fisher J, Suh H, Harada H, Malynn BA, Korsmeyer SJ. Essential role of BAX, BAK in B cell homeostasis and prevention of autoimmune disease. PNAS. 2005; 102:11272–11277. [PubMed: 16055554]
22. Wei MC, Zong WX, Cheng EH, Lindsten T, Panoutsakopoulou V, Ross AJ, Roth KA, MacGregor GR, Thompson CB, Korsmeyer SJ. Proapoptotic BAX and BAK: a requisite gateway to mitochondrial dysfunction and death. Science. 2001; 292:727–730. [PubMed: 11326099]
23. White FA, Keller-Peck CR, Knudson CM, Korsmeyer SJ, Snider WD. Widespread elimination of naturally occurring neuronal death in *Bax*-deficient mice. J Neurosci. 1998; 18:1428–1439. [PubMed: 9454852]
24. Takeuchi O, Fisher J, Suh H, Harada H, Malynn BA, Korsmeyer SJ. Essential role of BAX,BAK in B cell homeostasis and prevention of autoimmune disease. Proc Natl Acad Sci U S A. 2005; 102:11272–11277. [PubMed: 16055554]
25. Zhang M, Xuan S, Bouxsein ML, von SD, Akeno N, Faugere MC, Malluche H, Zhao G, Rosen CJ, Efstratiadis A, Clemens TL. Osteoblast-specific knockout of the insulin-like growth factor (IGF) receptor gene reveals an essential role of IGF signaling in bone matrix mineralization. J Biol Chem. 2002; 277:44005–44012. [PubMed: 12215457]
26. Rodda SJ, McMahon AP. Distinct roles for Hedgehog and canonical Wnt signaling in specification, differentiation and maintenance of osteoblast progenitors. Development. 2006; 133:3231–3244. [PubMed: 16854976]
27. Powell WF Jr. Barry KJ, Tulum I, Kobayashi T, Harris SE, Bringhurst FR, Pajevic PD. Targeted ablation of the PTH/PTHrP receptor in osteocytes impairs bone structure and homeostatic calcemic responses. J Endocrinol. 2011; 209:21–32. [PubMed: 21220409]
28. Livak KJ, Schmittgen TD. Analysis of relative gene expression data using real-time quantitative PCR and the $2^{-\Delta\Delta C}$T method. Methods. 2001; 25:402–408. [PubMed: 11846609]
29. Paic F, Igwe JC, Nori R, Kronenberg MS, Franceschetti T, Harrington P, Kuo L, Shin DG, Rowe DW, Harris SE, Kalajzic I. Identification of differentially expressed genes between osteoblasts and osteocytes. Bone. 2009; 45:682–692. [PubMed: 19539797]
30. Stephens A, Stephens S, Morrison N. Internal control genes for quantitative RT-PCR expression analysis in mouse osteoblasts, osteoclasts and macrophages. BMC Research Notes. 2011; 4:410. [PubMed: 21996334]
31. O'Brien CA, Jilka RL, Fu Q, Stewart S, Weinstein RS, Manolagas SC. IL-6 is not required for parathyroid hormone stimulation of RANKL expression, osteoclast formation, and bone loss in mice. Am J Physiol Endocrinol Metab. 2005; 289:E784–E793. [PubMed: 15956054]
32. Jilka RL, Almeida M, Ambrogini E, Han L, Roberson PK, Weinstein RS, Manolagas SC. Decreased oxidative stress and greater bone anabolism in the aged, when compared to the young, murine skeleton with parathyroid hormone administration. Aging Cell. 2010; 9:851–867. [PubMed: 20698835]
33. Glatt V, Canalis E, Stadmeyer L, Bouxsein ML. Age-related changes in trabecular architecture differ in female and male C57BL/6J mice. J Bone Miner Res. 2007; 22:1197–1207. [PubMed: 17488199]
34. Bouxsein ML, Boyd SK, Christiansen BA, Guldberg RE, Jepsen KJ, Muller R. Guidelines for assessment of bone microstructure in rodents using micro-computed tomography. J Bone Miner Res. 2010; 25:1468–1486. [PubMed: 20533309]
35. Schneider P, Stauber M, Voide R, Stampanoni M, Donahue LR, Muller R. Ultrastructural properties in cortical bone vary greatly in two inbred strains of mice as assessed by synchrotron light based micro- and nano-CT. J Bone Miner Res. 2007; 22:1557–1570. [PubMed: 17605631]
36. Dempster DW, Compston JE, Drezner MK, Glorieux FH, Kanis JA, Malluche H, Meunier PJ, Ott SM, Recker RR, Parfitt AM. Standardized nomenclature, symbols, and units for bone histomorphometry: A update of the report of the ASBMR Histomorphometry Nomenclature Committee. J Bone Miner Res. 2013; 28:2–17. [PubMed: 23197339]
37. Barragan-Adjemian C, Nicolella D, Dusevich V, Dallas MR, Eick JD, Bonewald LF. Mechanism by which MLO-A5 late osteoblasts/early osteocytes mineralize in culture: similarities with mineralization of lamellar bone. Calcif Tissue Int. 2006; 79:340–353. [PubMed: 17115241]

38. Feng JQ, Ward LM, Liu S, Lu Y, Xie Y, Yuan B, Yu X, Rauch F, Davis SI, Zhang S, Rios H, Drezner MK, Quarles LD, Bonewald LF, White KE. Loss of DMP1 causes rickets and osteomalacia and identifies a role for osteocytes in mineral metabolism. Nat Genet. 2006; 38:1310–1315. [PubMed: 17033621]
39. Almeida M, Ambrogini E, Han L, Manolagas SC, Jilka RL. Increased lipid oxidation causes oxidative stress, increased PPARγ expression and diminished pro-osteogenic Wnt signaling in the skeleton. J Biol Chem. 2009; 284:27438–27448. [PubMed: 19657144]
40. Davey RA, Clarke MV, Sastra S, Skinner JP, Chiang C, Anderson PH, Zajac JD. Decreased body weight in young Osterix-Cre transgenic mice results in delayed cortical bone expansion and accrual. Transgenic Res. 2012; 21:885–893. [PubMed: 22160436]
41. Jilka RL, Weinstein RS, Bellido T, Roberson P, Parfitt AM, Manolagas SC. Increased bone formation by prevention of osteoblast apoptosis with parathyroid hormone. J Clin Invest. 1999; 104:439–446. [PubMed: 10449436]
42. Halloran BP, Ferguson VL, Simske SJ, Burghardt A, Venton LL, Majumdar S. Changes in bone structure and mass with advancing age in the male C57BL/6J mouse. J Bone Miner Res. 2002; 17:1044–1050. [PubMed: 12054159]
43. Pantschenko AG, Zhang W, Nahounou M, McCarthy MB, Stover ML, Lichtler AC, Clark SH, Gronowicz GA. Effect of osteoblast-targeted expression of Bcl-2 in bone: differential response in male and female mice. J Bone Miner Res. 2005; 20:1414–1429. [PubMed: 16007339]
44. Moriishi T, Maruyama Z, Fukuyama R, Ito M, Miyazaki T, Kitaura H, Ohnishi H, Furuichi T, Kawai Y, Masuyama R, Komori H, Takada K, Kawaguchi H, Komori T. Overexpression of Bcl2 in osteoblasts inhibits osteoblast differentiation and induces osteocyte apoptosis. PLoS ONE. 2011; 6:e27487. [PubMed: 22114675]
45. Weiss A, Arbell I, Steinhagen-Thiessen E, Silbermann M. Structural changes in aging bone: osteopenia in the proximal femurs of female mice. Bone. 1991; 12:165–172. [PubMed: 1910958]
46. Silbermann M, Weiss A, Reznick AZ, Eilam Y, Szydel N, Gershon D. Age-related trend for osteopenia in femurs of female C57BL/6 mice. Compr Gerontol [A]. 1987; 1:45–51.
47. Ferguson VL, Ayers RA, Bateman TA, Simske SJ. Bone development and age-related bone loss in male C57BL/6J mice. Bone. 2003; 33:387–398. [PubMed: 13678781]
48. Boyde A, Compston JE, Reeve J, Bell KL, Noble BS, Jones SJ, Loveridge N. Effect of estrogen suppression on the mineralization density of iliac crest biopsies in young women as assessed by backscattered electron imaging. Bone. 1998; 22:241–250. [PubMed: 9514216]
49. Enlow DH. A study of the post-natal growth and remodeling of bone. Am J Anat. 1962; 110:79–101. [PubMed: 13890322]
50. Bellido T, Ali AA, Plotkin LI, Fu Q, Gubrij I, Roberson PK, Weinstein RS, O'Brien CA, Manolagas SC, Jilka RL. Proteasomal degradation of Runx2 shortens parathyroid hormone-induced anti-apoptotic signaling in osteoblasts: a putative explanation for why intermittent administration is needed for bone anabolism. J Biol Chem. 2003; 278:50259–50272. [PubMed: 14523023]
51. Wan M, Yang C, Li J, Wu X, Yuan H, Ma H, He X, Nie S, Chang C, Cao X. Parathyroid hormone signaling through low-density lipoprotein-related protein 6. Genes Dev. 2008; 22:2968–2979. [PubMed: 18981475]
52. Kramer I, Keller H, Leupin O, Kneissel M. Does osteocytic SOST suppression mediate PTH bone anabolism? Trends Endocrinol Metab. 2010; 21:237–244. [PubMed: 20074973]
53. Almeida M, Iyer S, Martin-Millan M, Bartell SM, Han L, Ambrogini E, Onal M, Xiong J, Weinstein RS, Jilka RL, O'Brien CA, Manolagas SC. Estrogen receptor-alpha signaling in osteoblast progenitors stimulates cortical bone accrual. J Clin Invest. 2013; 123:394–404. [PubMed: 23221342]
54. Jilka RL, O'Brien CA, Ali AA, Roberson PK, Weinstein RS, Manolagas SC. Intermittent PTH stimulates periosteal bone formation by actions on post-mitotic preosteoblasts. Bone. 2009; 44:275–286. [PubMed: 19010455]
55. Parfitt, AM.; Kleerekoper, M.; Villanueva, AR. Increased bone age: Mechanisms and consequences. In: Christianson, J.; Johnsen, C.; Riis, BJ., editors. Osteoporosis. Osteopress ApS, Copenhagen: 1987. p. 301-308.

56. Shimizu S, Kanaseki T, Mizushima N, Mizuta T, Arakawa-Kobayashi S, Thompson CB, Tsujimoto Y. Role of Bcl-2 family proteins in a non-apoptotic programmed cell death dependent on autophagy genes. Nat Cell Biol. 2004; 6:1221–1228. [PubMed: 15558033]
57. Manolagas SC, Parfitt AM. For whom the bell tolls: osteocyte distress signals and the pathogenesis of metabolic bone diseases. Bone. 2013; 54:272–278. [PubMed: 23010104]
58. Lloyd SA, Yuan YY, Kostenuik PJ, Ominsky MS, Lau AG, Morony S, Stolina M, Asuncion FJ, Bateman TA. Soluble RANKL induces high bone turnover and decreases bone volume, density, and strength in mice. Calcif Tissue Int. 2008; 82:361–372. [PubMed: 18465074]
59. Yuan YY, Kostenuik PJ, Ominsky MS, Morony S, Adamu S, Simionescu DT, Basalyga DM, Asuncion FJ, Bateman TA. Skeletal deterioration induced by RANKL infusion: a model for high-turnover bone disease. Osteoporos Int. 2008; 19:625–635. [PubMed: 18038244]
60. Jilka RL, O'Brien CA, Weinstein RS, Manolagas SC. Continuous elevation of PTH increases the number of osteoblasts via both osteoclast-dependent and - independent mechanisms. J Bone Miner Res. 2010; 25:2427–2437. [PubMed: 20533302]
61. Jilka, RL.; Bellido, T.; Almeida, M.; Plotkin, LI.; O'Brien, C.; Weinstein, RS.; Manolagas, SC. Apoptosis of Bone Cells. In: Bilezikian, JP.; Raisz, LG.; Martin, T., editors. Principles of Bone Biology. 3rd ed.. Academic Press; 2008. p. 235-259.

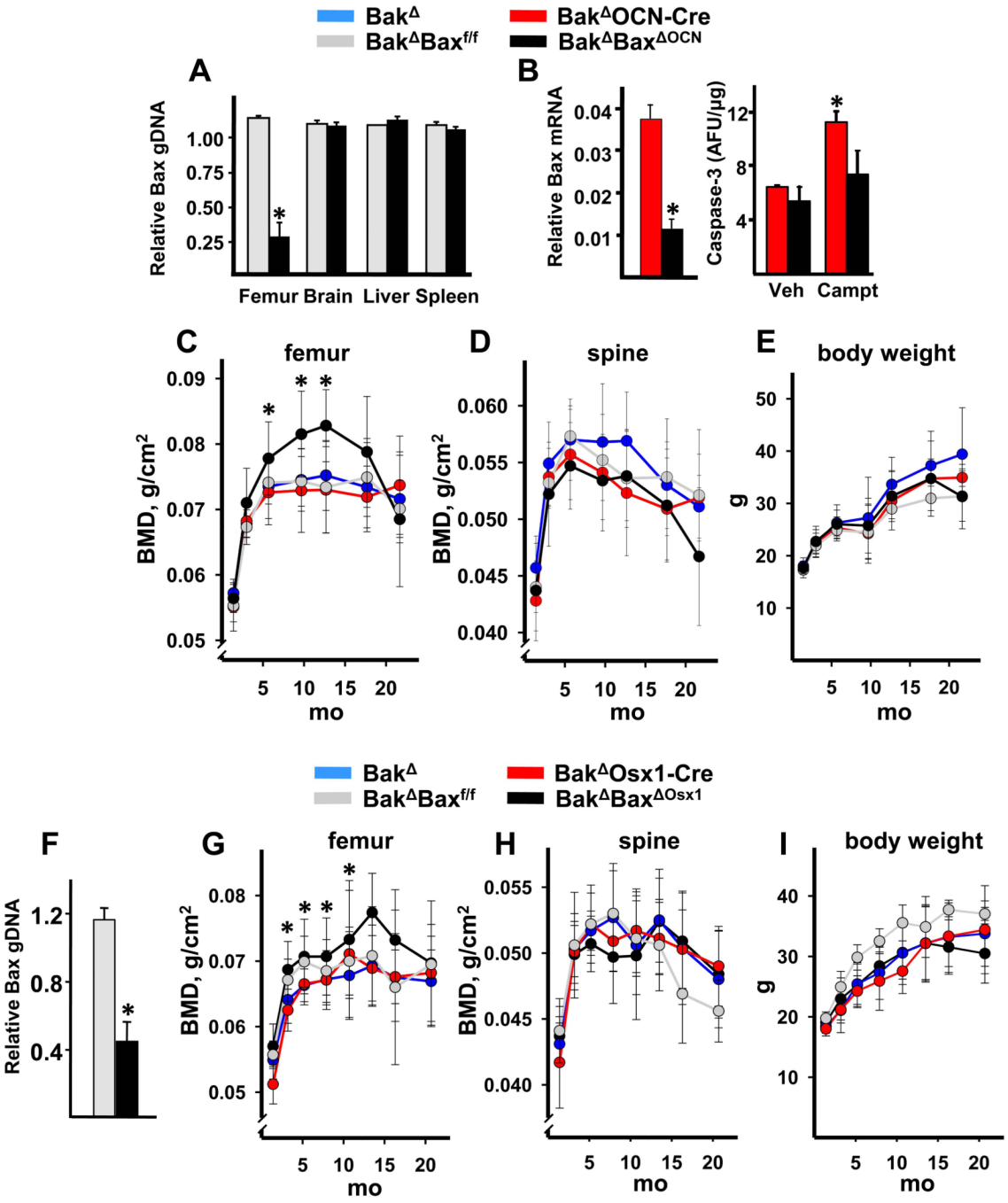

Figure 1. Deletion of Bak and Bax increases femoral bone mass

(A–E) Experiments with the OCN-Cre deleter strain. (**A**) Level of Bax genomic DNA in osteocyte-enriched femoral shafts, brain, spleen or liver from 3-month-old female mice; n=5 animals per group; **p* <0.05 vs. $Bak^{\Delta}Bax^{f/f}$. (**B**) Bax expression (left panel) and caspase-3 activity (right panel) in triplicate cultures of osteoblastic cells established from marrow-derived progenitors of 3-month-old female mice. Caspase-3 activity was determined 8 hours following addition of vehicle (Veh) or 0.2 μM camptothecin (Campt), **p*<0.05. Sequential determination of femoral BMD (**C**) spinal BMD (**D**), and body weight (**E**) in a cohort of female mice; n=9–14/group. **p*<0.05 vs. littermate controls by random coefficients model.

(F–I) Experiments with the Osx1-Cre deleter strain. (**A**) Level of Bax genomic DNA in osteocyte-enriched femoral shafts from 2-month-old female mice; n=3 animals per group; *p<0.05 vs. $Bak^{\Delta};Bax^{f/f}$. Sequential determination of femoral BMD **(G)**, spinal BMD **(H)** and body weight **(I)** in a cohort of female mice; n=6–11/group, *p<0.05 vs. Bak^{Δ} and BakΔOsx1-Cre littermate controls by random coefficients model.

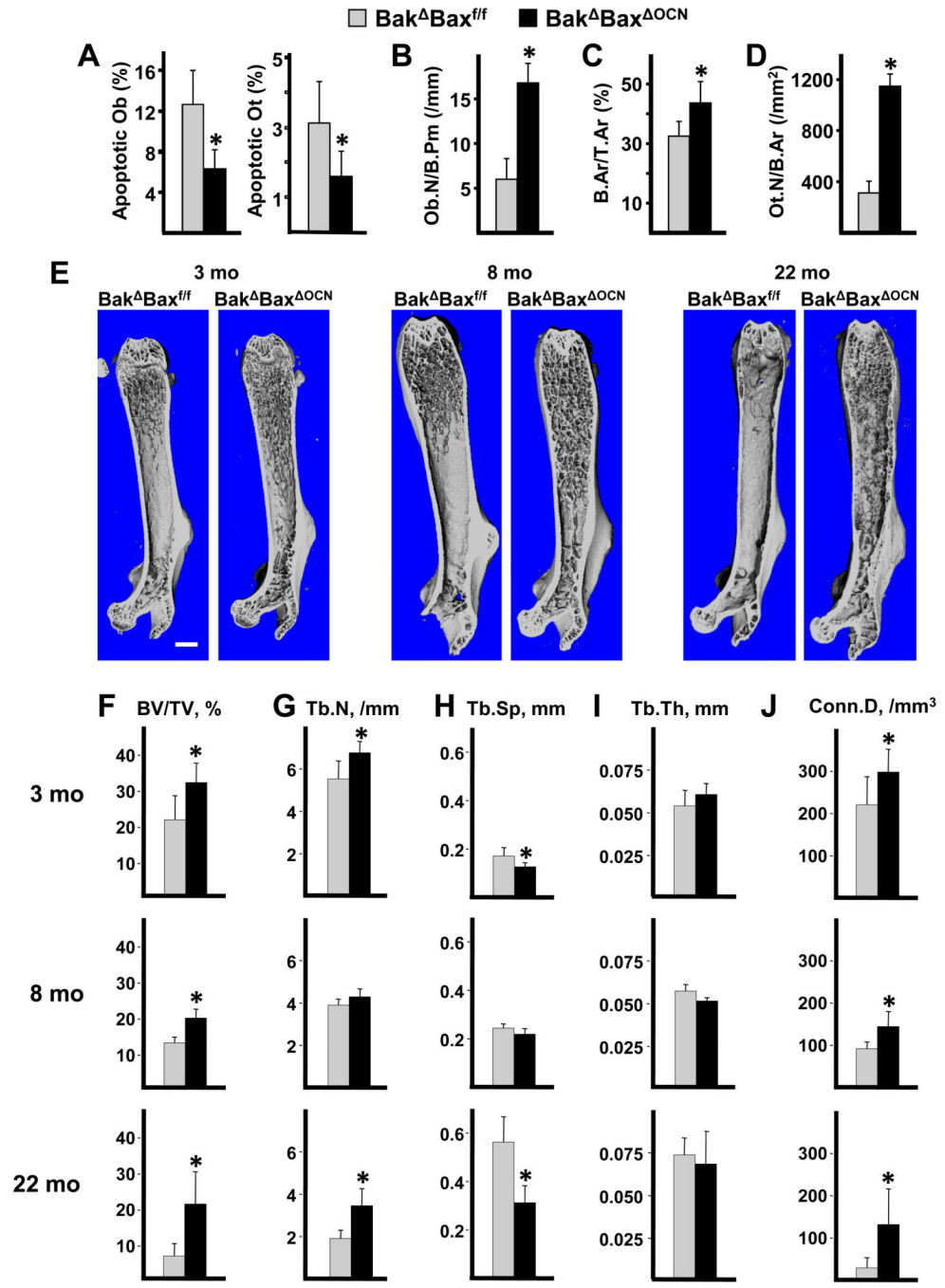

Figure 2. Deletion of Bax with OCN-Cre reduces osteoblast and osteocyte apoptosis and increases femoral cancellous bone mass

Histomorphometric determination of cancellous osteoblast (Ob) apoptosis, and cortical osteocyte (Ot) apoptosis (**A**); as well as cancellous osteoblast number (**B**), cancellous bone area (**C**), and osteocyte density (**D**) in femoral sections from 8-month-old male mice, n=4–5/group. **(E)** Representative micro-CT images of femora from Bak$^{\Delta}$Bax$^{f/f}$ and Bak$^{\Delta}$Bax$^{\Delta OCN}$ littermates; scale bar, 1 mm. Micro-CT was used to image and quantify femoral bone from 3-month-old mice comprising 2 males and 4 females of each genotype, 8-month-old male mice, and 22-month-old female mice. Micro-CT determination of trabecular bone volume (BV/TV) (**F**), trabecular number (Tb.N) (**G**), trabecular separation (Tb.Sp) (**H**), trabecular

thickness (Tb.Th) (**I**) and connectivity density (Conn.D) (**J**) in the distal metaphysis of femora from $Bak^{\Delta}Bax^{f/f}$ mice at 3 months (n=6), 8 months (n = 7) or 22 months (n = 8) of age; and from $Bak^{\Delta}Bax^{\Delta OCN}$ mice at 3 months (n = 6) , 8 months (n = 5) or 22 months (n = 9). *p <0.05 vs. $Bak^{\Delta}Bax^{f/f}$ littermates.

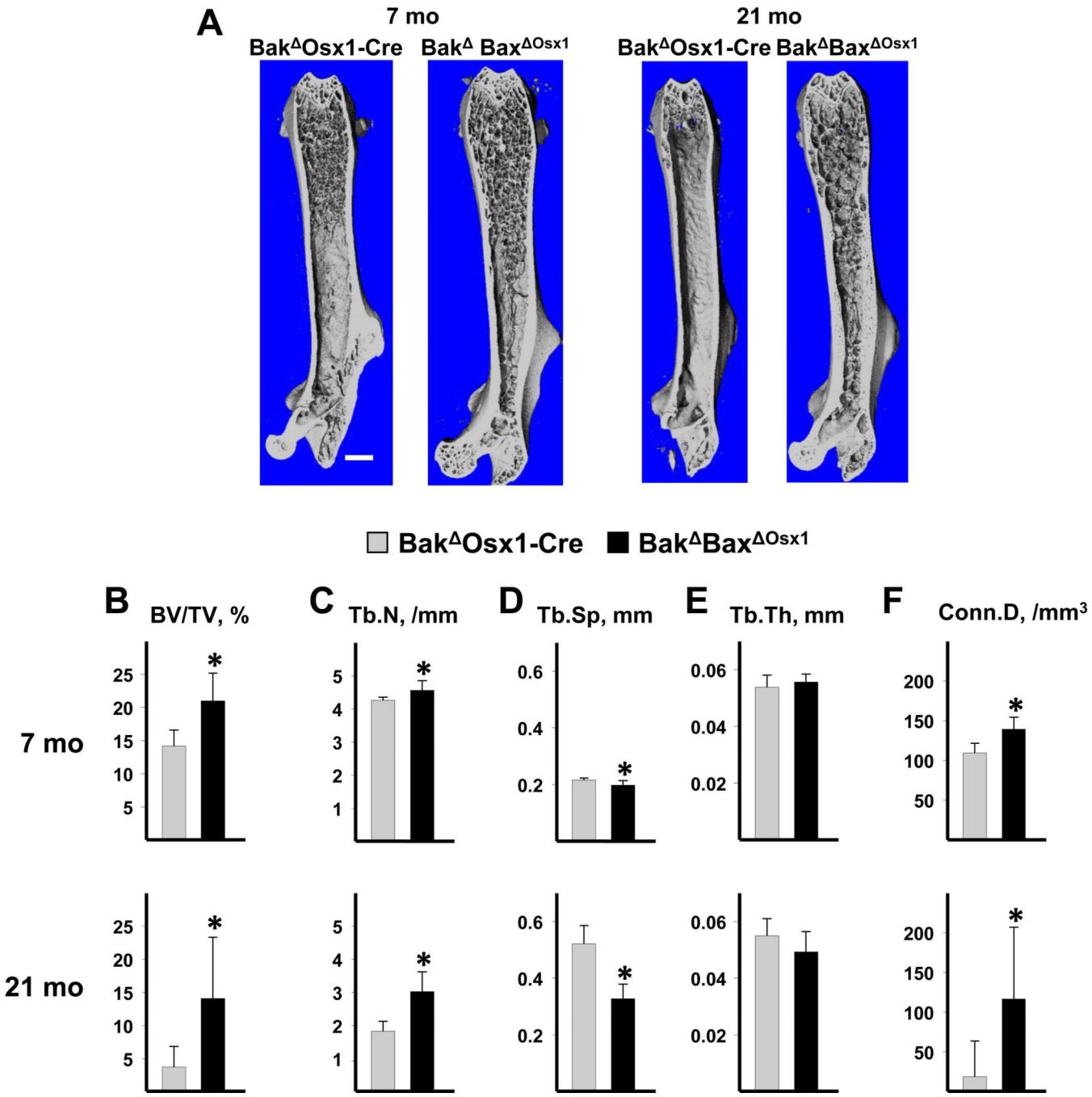

Figure 3. Deletion of Bak and Bax with Osx1-Cre increases femoral cancellous bone mass

(A) Representative micro-CT images from Bak$^{\Delta}$Bax$^{\Delta Osx1}$ and Bak$^{\Delta}$Osx1-Cre littermates at 7 months of age in males, and at 21 months of age in females. Scale bar, 1mm. Micro-CT determination of trabecular bone volume (BV/TV) (**B**), trabecular number (Tb.N) (**C**), trabecular separation (Tb.Sp) (**D**), trabecular thickness (Tb.Th) (**E**) and connectivity density (Conn.D) (**F**) in the distal metaphysis of femora from Bak$^{\Delta}$Osx1-Cre mice at 7 months of age (n = 9) and 21 months of age (n = 7); and Bak$^{\Delta}$Osx1-Cre mice at 7 months of age (n = 8) and 21 months of age (n = 9). *p<0.05 vs. Bak$^{\Delta}$Osx1-Cre littermates.

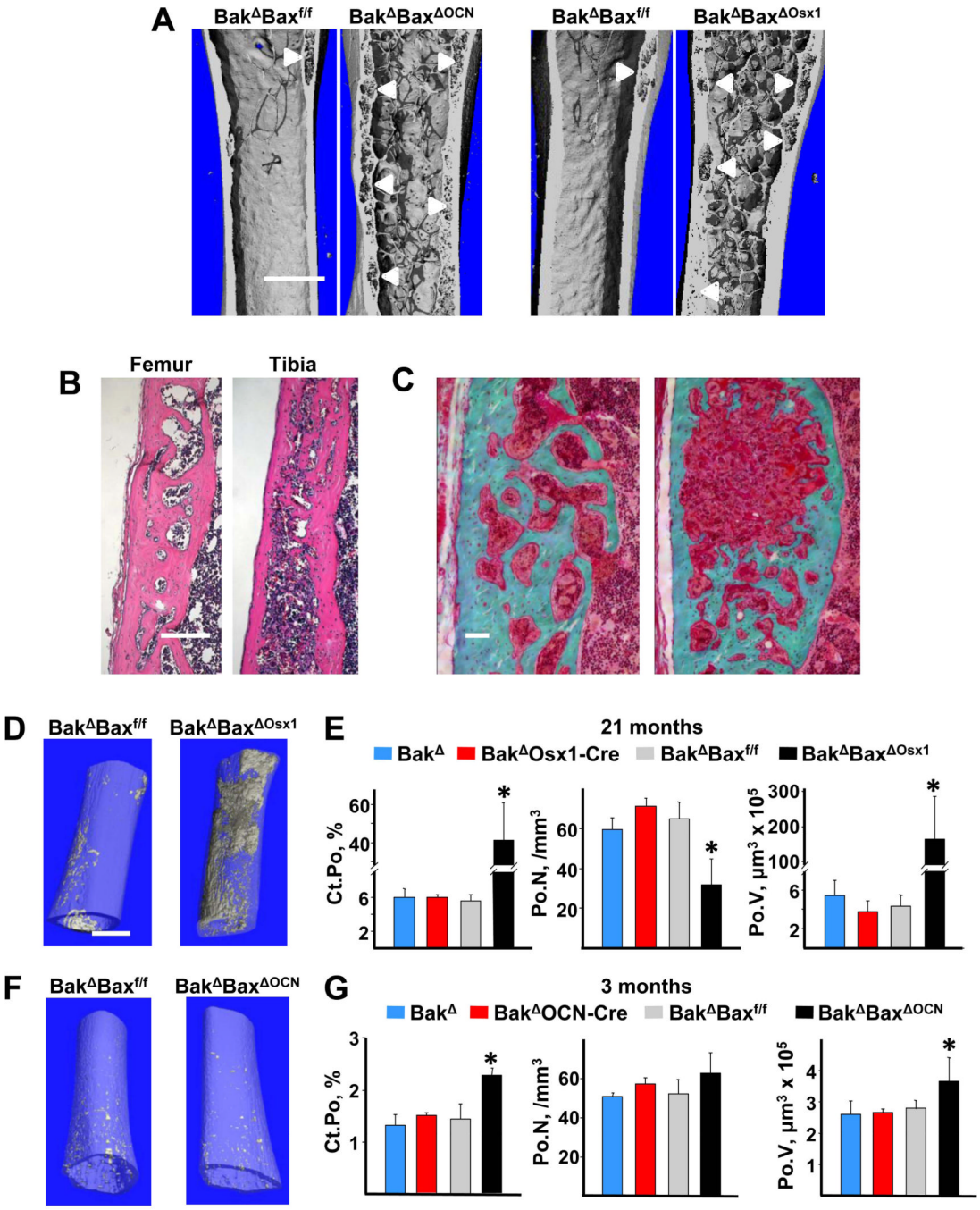

Figure 4. Lack of Bax and Bak increases cortical porosity in aged mice

(**A**) Representative micro-CT images of femora from 22-month-old female $Bak^{\Delta}Bax^{\Delta OCN}$ and $Bak^{\Delta}Bax^{f/f}$ littermates (left panel), and 21-month-old female $Bak^{\Delta}Bax^{\Delta Osx1}$ and $Bak^{\Delta}Bax^{f/f}$ littermates (right panel), scale bar, 1 mm. White arrowheads mark location of pores in cortical bone. (**B**) Representative femoral and tibial H&E-stained decalcified sections from 21-month-old female $Bak^{\Delta}Bax^{\Delta Osx1}$ mice, with the periosteal surface on the left; scale bar, 1 mm. (**C**) Representative femoral Trichrome-stained nondecalcified sections of femoral cortex from 22-month-old female $Bak^{\Delta}Bax^{\Delta OCN}$ mice, with the periosteal surface on the left.; scale bar, 50 μm. **(D)** Inverse micro-CT images of the distal half of femora from

21-month-old female mice. Void areas are depicted in grey within a transparent bone matrix. (**E**) Cortical porosity (Ct.Po), pore number (Po.N) and pore volume (Po.V) in the cortex of the distal half of femora from 21-month-old female mice, n=3–4/group. **(F)** Inverse micro-CT images of the distal half of femora from 3-mo-old female mice. (**G**) Porosity, pore number and pore volume in 3-month-old female mice, n=3/group, *$p<0.05$ vs. littermate controls.

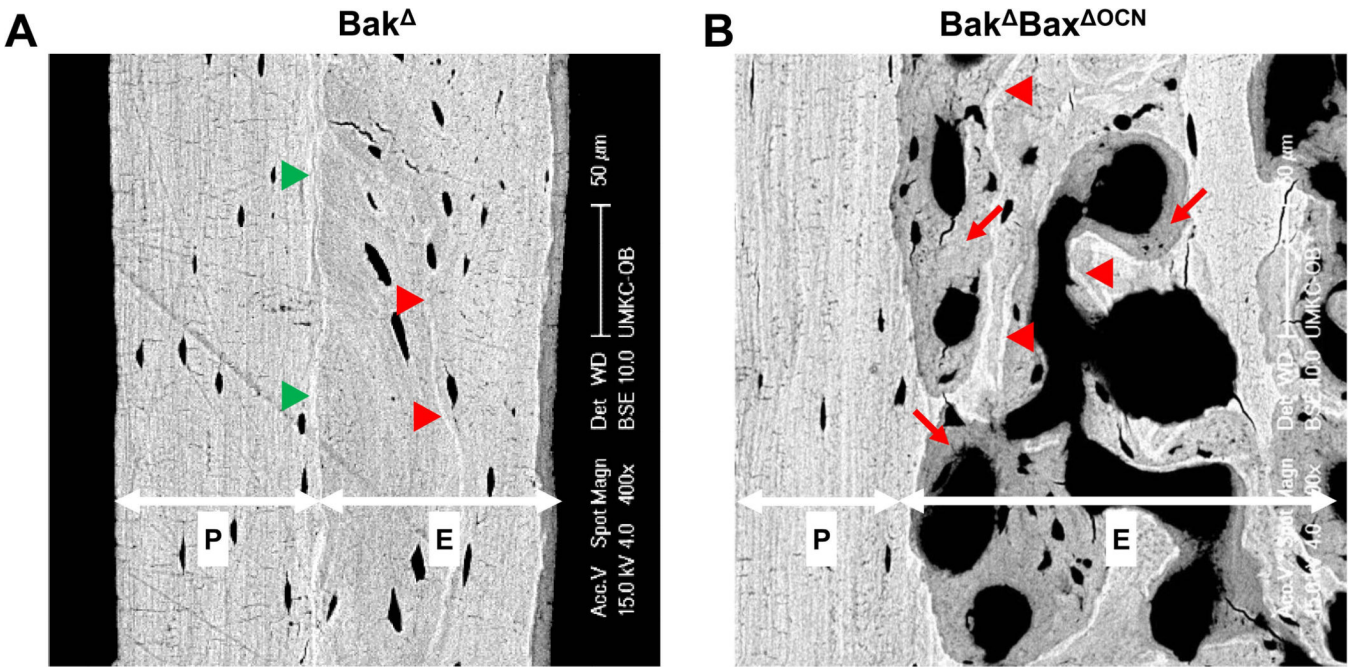

Figure 5. Increased cortical porosity of aged Bak$^{\Delta}$Bax$^{\Delta OCN}$ mice is restricted to the endosteal zone

Representative BSEM images of the femoral diaphyseal cortex from **(A)** a 22-month-old female Bak$^{\Delta}$ mouse, and **(B)** a 22-month-old female Bak$^{\Delta}$Bax$^{\Delta OCN}$ mouse. Endosteal ("E") and periosteal ("P") zones are separated by a highly mineralized boundary, indicated by green arrowheads. Red arrowheads mark highly mineralized cement lines that reflect previous remodeling activity. Red arrows denote areas of recently remodeled bone that have not yet achieved full mineralization.

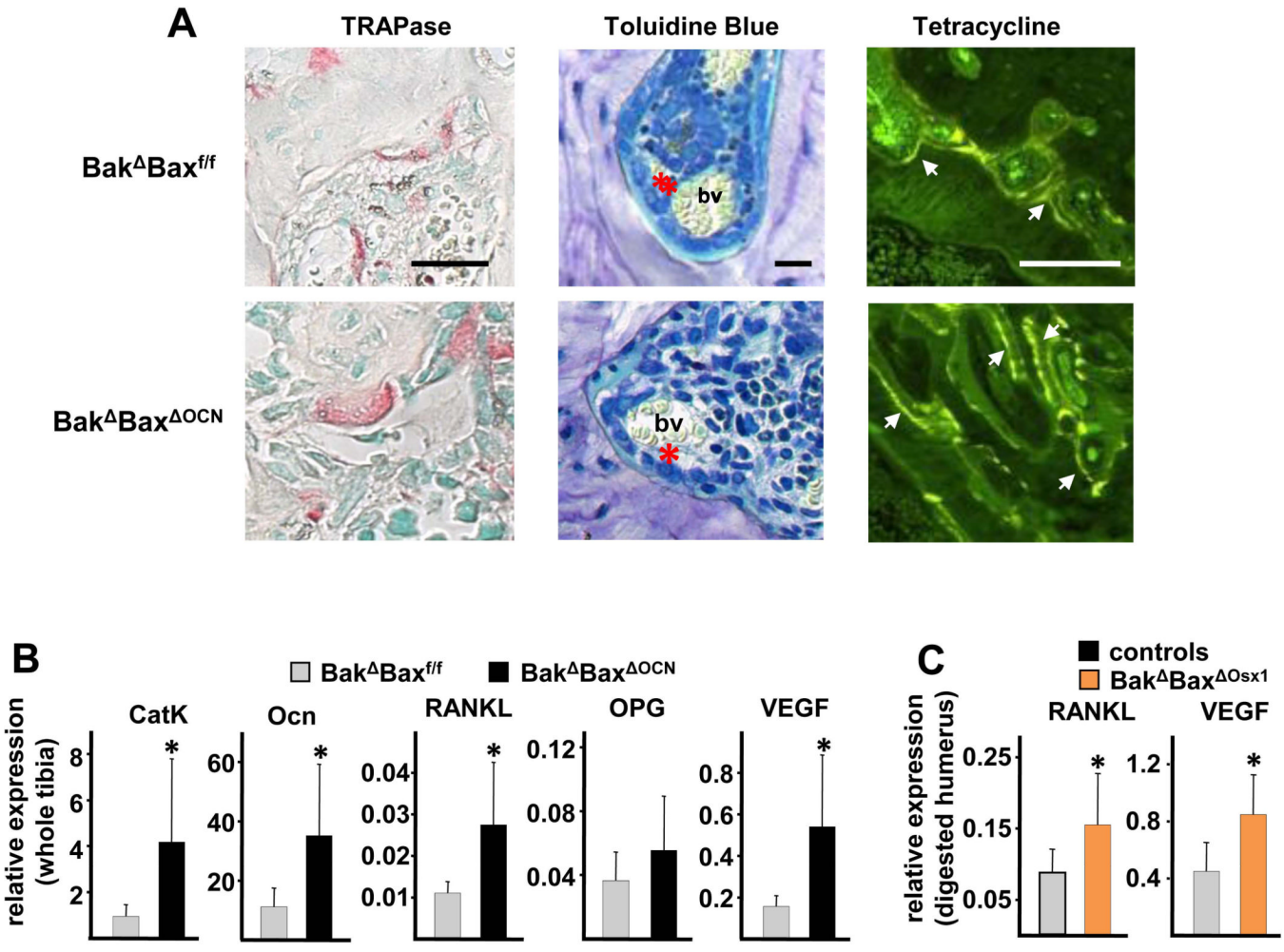

Figure 6. The age-related increase in porosity in Bak/Bax-deficiency is associated with intracortical bone remodeling and increased expression of RANKL and VEGF by osteocytes

(A) Femoral bone sections from 22-month-old female mice were stained for TRAPase to visualize osteoclasts, stained red (left panels); with toluidine blue (middle panels) to view osteoblasts (red asterisk) and blood vessels (bv); or viewed with fluorescence microscopy (right panels) to observe tetracycline labeling (arrow heads). scale bar, 10 μm (left and middle panels) or 100 μm (right panels). (**B**) Cathepsin K (CatK), osteocalcin (Ocn), RANKL, OPG and VEGF mRNA levels in whole tibiae from 22-month-old female mice (n=8–10/group) *p<0.05 vs. Bak$^{\Delta}$Bax$^{f/f}$ littermates. (**C**) RANKL and VEGF mRNA levels in collagenase-digested humeri, enriched in osteocytes, from 21-month-old female mice, n=6–7/group; *p<0.05 vs. combined littermate controls.

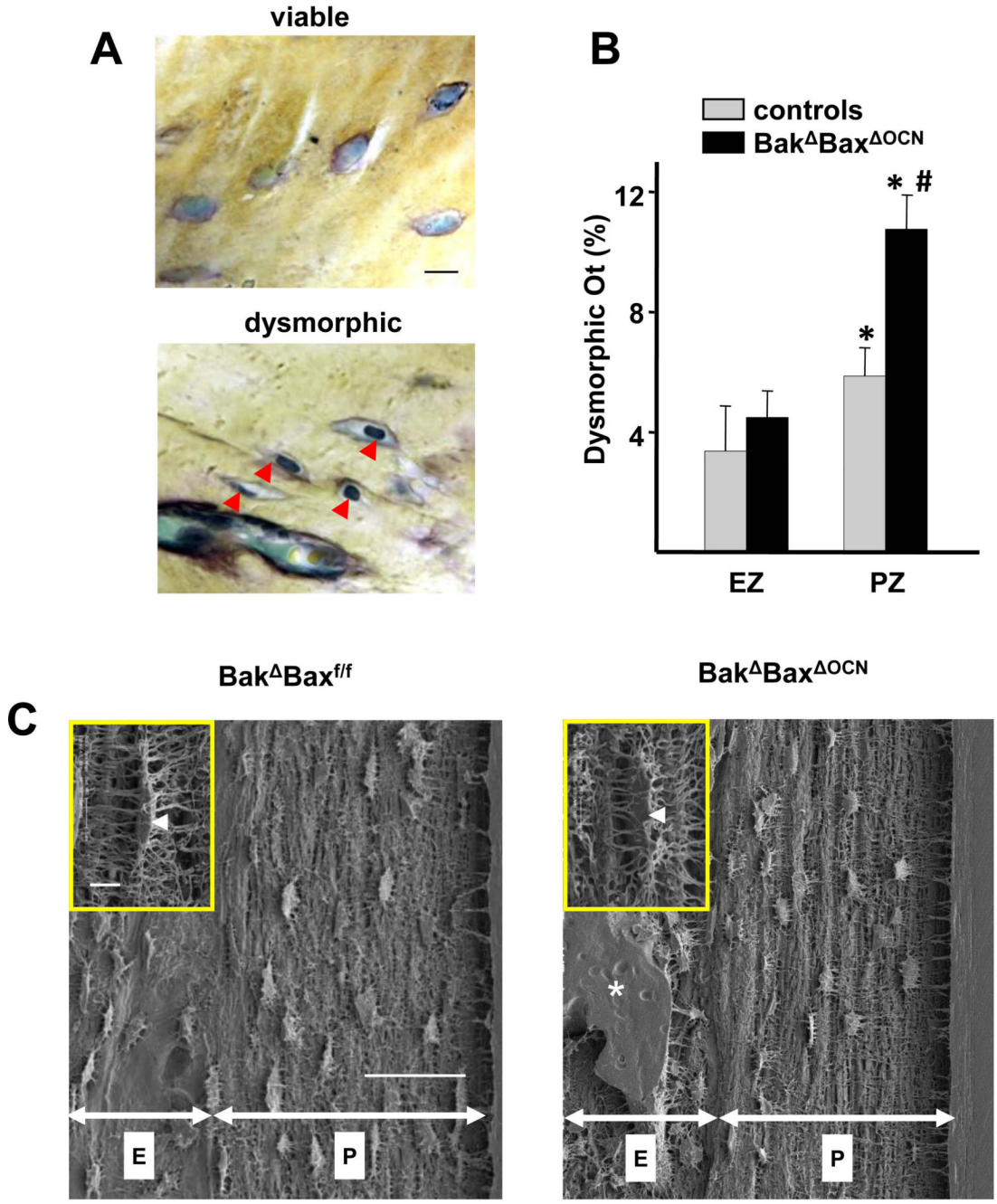

Figure 7. Increased prevalence of dysmorphic osteocytes is associated with increased porosity of aged Bak$^{\Delta}$Bax$^{\Delta OCN}$ mice

(**A**) Representative histologic nondecalcified sections showing viable osteocytes with typical morphology (upper panel) and dysmorphic osteocytes (red arrow heads, lower panel) in the periosteal zone of the femoral cortex from 22-month-old female mice. Scale bar, 10μm. (**B**) The percentage of dysmorphic osteocytes in endosteal (EZ) and periosteal (PZ) zones of the cortex of 22-mo-old female mice, n=7–8/group. *p<0.05 vs. EZ; #p<0.05 vs. PZ of combined controls. (**C**) Lacunar and canalicular morphology of cortical osteocytes of 22-month-old mice in the endosteal (“E”) and periosteal (“P”) zones, visualized by acid-etch

SEM. Scale bar, 50 μm. Inset: high magnification image of typical lacuna (arrowhead) and canaliculi in the periosteal zone. Scale bar 5 μm; *, cortical void.

Table 1

Deletion of Bak and Bax increases cortical porosity in the femur and tibia in aged female mice.

A. OCN-Cre model (22 months old)

	Porosity, % (N)			
	Bak^{Δ}	**$Bak^{\Delta}Bax^{f/f}$**	**Bak^{Δ}OCN-Cre**	**$Bak^{\Delta}Bax^{\Delta OCN}$**
Femur	4.7 ± 1.4 (2)	3.6 ± 4.7 (3)	11.4 ± 8.3 (4)	23.3 ± 11.5 (7)[a]
Tibiae	4.1 ± 4.1 (7)	6.4 ± 3.1 (5)	6.2 ± 5.2 (9)	27.2 ± 16.5 (4)[b]

B. Osx1-Cre model (21 months old)

	Porosity, % (N)			
	Bak^{Δ}	**$Bak^{\Delta}Bax^{f/f}$**	**Bak^{Δ}Osx1-Cre**	**$Bak^{\Delta}Bax^{\Delta Osx1}$**
Femur	2.1 ± 0.9 (4)	NA	4.7 ± 1.2 (3)	19.2 ± 6.8 (4)[b]
Tibiae	4.1 ± 2.2 (6)	3.2 ± 1.6 (3)	3.3 ± 2.9 (7)	16.6 ± 7.1 (6)[b]

NA, none available for measurement;

[a] $p < 0.05$ vs. Bak^{Δ} and $Bak^{\Delta}Bax^{f/f}$, $p = 0.06$ vs. Bak^{Δ}OCN-Cre,

[b] $p < 0.05$ vs. littermate controls. Numbers in parentheses are the number of samples.

Table 2

Increased intracortical bone engaged in remodeling in aged $Bak^{\Delta}Bax^{\Delta OCN}$ mice.

	Intracortical		Cancellous	
	controls	**$Bak^{\Delta}Bax^{\Delta OCN}$**	**controls**	**$Bak^{\Delta}Bax^{\Delta OCN}$**
B.Pm (mm)*	11.4 ± 7.2	42.3 ± 13.4[a]	3.13 ± 1.55	17.6 ± 8.4[a]
Vo.Ar/EZ.Ar	0.10 ± 0.10	0.33 ± 0.22[a]	-	-
B.Ar/T.Ar	-	-	0.012 ± 0.006	0.061 ± 0.037[a]
Oc.Pm (mm)*	0.47 ± 0.38	1.48 ± 0.80[a]	0.19 ± 0.26	0.89 ± 1.21
Oc.Pm/B.Pm	0.036 ± 0.024	0.034 ± 0.012	0.055 ± 0.050	0.037 ± 0.038
Oc.N/B.Pm (/mm)	1.15 ± 0.75	1.10 ± 0.49	2.25 ± 2.13	1.65 ± 1.85
M.Pm/B.Pm	0.24 ± 0.08	0.21 ± 0.02	0.22 ± 0.06	0.17 ± 0.06
MAR (μm/d)	1.64 ± 0.20	1.28 ± 0.22	1.34 ± 0.24	1.23 ± 0.09
BFR/BS ($\mu m^2/\mu m/d$)	0.34 ± 0.08	0.25 ± 0.06	0.30 ± 0.12	0.20 ± 0.08

B.Pm = bone perimeter; Vo.Ar/EZ.Ar = intracortical void area fraction of endosteal zone area; B.Ar/T.Ar = cancellous bone fraction of tissue area; Oc.Pm = osteoclast perimeter; Oc.Pm/B.Pm = osteoclast perimeter fraction of bone perimeter; Oc.N/B.Pm = osteoclast number per bone perimeter; M.Pm/B.Pm = mineralizing fraction of bone perimeter; MAR = mineral apposition rate; BFR/BS = bone formation rate.

*These measurements are unadjusted values, used here to indicate the increased perimeter available in $Bak^{\Delta}Bax^{\Delta OCN}$ mice. Data from female $Bak^{\Delta}Bax^{\Delta OCN}$ mice (n = 6) and combined female littermate controls (n = 9) are shown;

[a] $p<0.05$ vs. controls.

Table 3

Calcium homeostasis in 21-month-old female mice is unaffected by deletion of Bak and Bax.

	Bak^{Δ}	$Bak^{\Delta}Bax^{f/f}$	Bak^{Δ}Osx1-Cre	$Bak^{\Delta}Bax^{\Delta Osx1}$
calcium (mg/ml)	7.64 ± 0.53 (8)	8.22 ± 0.72 (3)	8.17 ± 0.43 (7)	7.86 ± 0.55 (8)
phosphate (mg/ml)	12.5 ± 2.3 (8)	16.5 ± 3.5 (3)	13.3 ± 5.0 (7)	14.3 ± 1.8 (8)
PTH (pg/ml)	216 ± 95 (8)	218 ± 164 (3)	219 ± 116 (7)	241 ± 189 (8)
Cyp27b1 mRNA (relative to GAPDH)	0.023 ± 0.019 (4)	0.025 ± 0.006 (3)	0.018 ± 0.008 (5)	0.024 ± 0.012 (5)

Numbers in parentheses are the number of samples.